Hindawi
Journal of Sensors
Volume 2019, Article ID 5184907, 11 pages
https://doi.org/10.1155/2019/5184907

Research Article

Selected Aging Effects in Triaxial MEMS Accelerometers

Sergiusz Łuczak, Maciej Zams, and Karol Bagiński

Warsaw University of Technology, Faculty of Mechatronics, Institute of Micromechanics and Photonics, Ul. Boboli 8, Warsaw 02-525, Poland

Correspondence should be addressed to Sergiusz Łuczak; sergiusz.luczak@pw.edu.pl

Received 29 March 2019; Revised 14 August 2019; Accepted 22 August 2019; Published 18 November 2019

Academic Editor: Pawel Malinowski

Copyright © 2019 Sergiusz Łuczak et al. This is an open access article distributed under the Creative Commons Attribution License, which permits unrestricted use, distribution, and reproduction in any medium, provided the original work is properly cited.

Natural aging of commercial triaxial low-g MEMS accelerometers, manufactured by surface micromachining, was evaluated in terms of changes of their offset voltages and scale factors, assigned to each sensitive axis. Two pieces of two models of triaxial accelerometers (ADXL 330 and ADXL 327 by Analog Devices Inc.) with analog outputs were tested within a period of ca. 4.5 years. Two different computer-controlled test rigs were used for performing relevant experimental studies, employing tilt angles as the reference source. Methodology of determining the proposed indicators of aging was based on cyclic repetition of the calibration procedure for each accelerometer. Changes of the output signals of the tested accelerometers were observed, resulting in respective indication errors of ca. 0.8% or even 2.2% while related to determining tilt. Since the accelerometers were operated under mild conditions while tested, much bigger errors are to be expected in the case of harsh conditions. Both pieces of ADXL 330 accelerometers ceased to operate properly within the testing period, approximately at the same time, for no apparent reason; thus, it is recommended to introduce redundancy in relevant reliable measuring circuits by doubling the number of the applied accelerometers.

1. Introduction

Since their introduction to the market as detectors in automotive airbag systems in the 1980s, Microelectromechanical System (MEMS) accelerometers have been employed in an ever-increasing number of mechatronic and electronic systems. Whereas some modern applications, e.g., in smartphones [1] and the like (tablets, photo cameras, and smartwatches [2]), may not be so strategic, there are other devices, e.g., automotive safety systems like the said airbag or a new generation of motorcycle ABS [3], or even diving instruments [4], where MEMS accelerometers are directly responsible for the protection of human life—then, the related aging effects become as critical as the results of aging of, e.g., social infrastructures such as bridges and other essential infrastructure systems [5]; health monitoring of such structures is a solution increasing safety of their users [6, 7].

In the case of such strategic applications, the lifetime of many devices with an embedded MEMS accelerometer may be quite long (especially due to their high cost), and thus, the aging phenomena in the accelerometer are of crucial importance. Moreover, micromachined accelerometers are sometimes the only alternative due to a demand for miniature dimensions.

In order to obtain possibly high accuracy, the output signals generated by MEMS accelerometers are often calibrated in very sophisticated ways, as reported, e.g., in [8–10]. Then, at the same time, the aging phenomena are compensated for [11]. However, if calibration was not repeated within a longer period of time, it would be advantageous to take into account errors due to aging and compensate for them.

As a rule, MEMS sensors feature worse metrological parameters compare to their conventional counterparts. In view of the limited amount of the published data, MEMS devices must often be experimentally tested in order to verify their usefulness in certain applications, which also applies to the problem of aging.

As proven by our own research, natural aging of two-axial MEMS accelerometers is quite an important issue, resulting in errors even up to 2.6% [12], yet very little data are provided in the related publications. Some companies as STMicroelectronics take into account the effects of aging,

designing sophisticated circuits controlling the accelerometers in such a way that some systematic errors related to aging phenomena are compensated for.

The aging phenomenon is also called "lifetime stability," "long-term reliability," or "drift over lifetime." Some manufacturers of MEMS accelerometers totally disregard it, whereas others guarantee that the data reported in respective data sheets are valid throughout the whole life of the accelerometer [13].

A survey of relevant publications does not provide a satisfying answer to the question of significance of aging effects in MEMS devices. Some publications report large errors due to aging, exceeding 5%, e.g., [14], while other authors claim that aging is insignificant, e.g., [15, 16]. Some researchers prove that aging trends in MEMS devices can be well predicted using exponential functions [17], whereas others state that such functions do not fit the real trends [18].

A conventional approach to studying aging effects is to perform accelerated tests, according to, e.g., ISO/IEC 60068-2, 60749-6 standard, or JESD22 series standards, where a MEMS device is subjected to vibration, high or low temperature, thermal and moisture cycling, etc. [19]. Accelerated testing may be realized as well by harsh electrical loading [20] or by subjecting the tested device to mechanical overloads. In the case of, e.g., PM sensors, accumulation of particles inside the measuring chamber may affect sensor aging, as well as meteorological conditions such as high humidity or extreme temperatures can affect the functioning of electronics of the device [21].

Despite the fact that lower temperatures and lower humidity levels result in longer life of MEMS [22], some authors question the reliability of accelerated testing in the case of MEMS, pointing only to humidity as the major factor accelerating the most of mechanical and electrical failures [23]. Such point of view can be proved by the results of a natural aging simulated by storing MEMS accelerometers at higher temperatures, when only small changes in their performance were reported in [24, 25]. As suggested in [26], it is crucial to distinguish between short-term and long-term degradation mechanisms in order to avoid a wrong lifetime prediction.

So, it may be stated that at this stage, the most reliable method of evaluating the considered effects is natural aging. For example, results of five different inertial measuring units (IMUs) containing MEMS accelerometers, tested over a period of 18 months, are reported in [27]. The observed changes were insignificant. However, many factors were involved here, as not only the accelerometers had been subjected to aging but the IMUs as a whole (including the circuits processing the output signals of the accelerometers).

The aging phenomena can be related to particular elements of MEMS accelerometer, i.e., mechanical components (the elastic suspension of the seismic mass), electric components (capacitive or piezoelectric transducers converting deflection of the elastic suspension or displacement of the seismic mass, into an electric quantity), electronic circuit (integrated with the mechanical structure on the same chip or created in a separate chip), and external electronic components setting operational parameters of the accelerometer (constant-voltage regulator, capacitors, and resistors).

Each of the aforementioned elements could be studied separately with regard to the effects of its aging. However, results of such study would be very complex and difficult to interpret in terms of overall effects. Thus, results presented in this study are not related to particular elements of the tested MEMS accelerometers but concern the entire accelerometer together with the basic electronic circuit (external capacitors and resistors, constant-voltage regulator) as a whole. Even though such approach has a general character, it is more convenient from a practical point of view. It evaluates the performance of the accelerometer as a whole device, which is more interesting for a potential user of such sensor.

2. Materials and Methods

While testing low-g accelerometers, the gravitational acceleration is a reference source featuring a satisfactory range of variation, when the accelerometer is tilted. As it is one of the most stable and accurate external reference sources available, it is commonly used in experimental studies of MEMS accelerometers, as reported, e.g., in [8, 10, 28, 29]. Generation of acceleration by means of standard or custom equipment, like, e.g., a nanopositioning stage used in experimental studies described in [30] or specialized equipment used in [31], is much more complicated and sometimes even less accurate.

2.1. The Tested Sensors. In order to evaluate the considered effects of aging taking place in triaxial MEMS accelerometers, it was decided to calibrate them using tilt angles (and thus the gravitational acceleration indirectly) as the reference. The calibration procedure was repeated many times (108 altogether) over a long-term period of more than 4.5 years (November 2013 to July 2018). The procedure consisted in changing and recording tilt of the tested accelerometer and then sampling its output signals at this angular position, which was always changed by rotating the accelerometer around only one of two horizontal axes at a time. As the accelerometers were triaxial sensors, the rotation axis was either pitch or roll axis (with no pitch involved). Two kinds of triaxial MEMS accelerometers by Analog Devices Inc., manufactured by surface micromachining, were tested: two pieces of ADXL 330 [32] (purchased in 2006) and two pieces of ADXL 327 [33] (purchased in 2011). Both pieces of each type were probably from the same production batch. The accelerometers were mounted on their PCB in 2011, thus had never been used before. The accelerometers are presented in Figure 1.

After the purchase (2006-2013) and within the whole time of testing (2013-2018), the tested accelerometers have been stored under laboratory conditions, with the ambient temperature in the range not exceeding 15-40°C (while calibrated, the range was 20-30°C; nevertheless, the accelerometer chips may have been subjected to higher temperatures due to internal ohmic losses; they were supplied with the voltage of 3 V by constant-voltage regulators operating at 5 V) and have never been subjected to mechanical overloads or shocks.

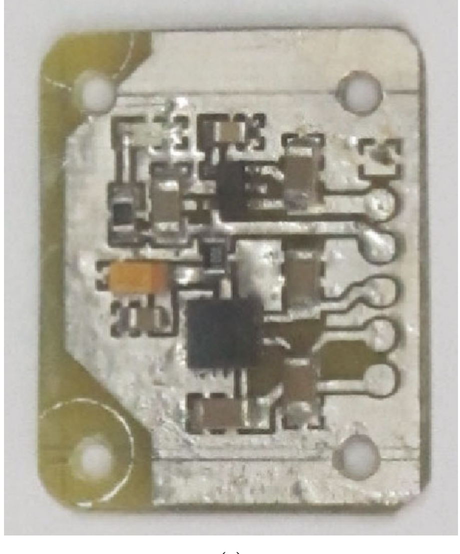

(a)

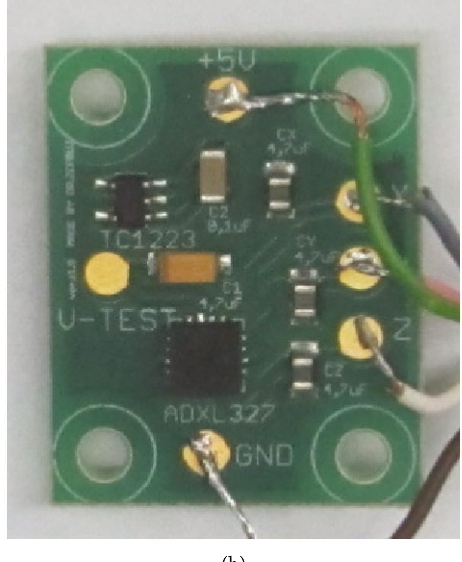

(b)

Figure 1: The tested accelerometers mounted on the PCB: (a) ADXL 330; (b) ADXL 327.

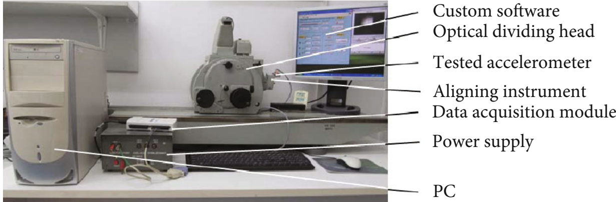

Figure 2: The test rig with the optical dividing head.

2.2. The Test Rigs. The accelerometers were tilted by means of two different test rigs. The main element of the first one, presented in Figure 2, was a manually driven optical dividing head, manufactured by Carl Zeiss Jena Company.

The output shaft of the dividing head, with the tested accelerometer mounted at one of two positions, is presented in Figure 3. As can be seen, the accelerometer PCB is attached to a special aligning instrument. The whole test rig and the aligning instrument have been minutely described by the author in [34, 35]. The dividing head was driven manually and enabled applying roll over the full angle with accuracy of ±0.0008°. It is also possible to apply a pitch angle of the output shaft over a smaller range; however, the shaft remained always leveled. The tested accelerometer was coupled with a data acquisition module NI 6211 by National Instruments, which was controlled by a PC (see Figure 2). It captured its three analog output voltage signals. Since only the roll angle was applied, in order to calibrate all the three sensitive axes of the tested accelerometers, two calibration procedures had to be completed, one with the accelerometer mounted as in Figure 3(a) and the other while mounted as in Figure 3(b).

The main elements of the second test rig, presented in Figure 4, were two rotary stages controlled by a PC. Each stage applied either pitch or roll, with accuracy of ±0.02° over the full angle. The mechanical structure of the test rig is quite typical and has been used in many similar research works, presented, e.g., in [36]. As in the case of the first test rig, the tested accelerometer was coupled with the same data acquisition module (NI 6211 by National Instruments). However, until November 2017, a PCI card was used for data acquisition (PCI 1716 by Advantech) instead of NI 6211. More detailed information about the test rig has been provided by the author in [37].

The data acquisition modules employed in both test rigs (PCI 1716, NI 6211) featured accuracy of ca. 0.0015 V [35, 38], with the error due to digital resolution included [39]. Application of two different test rigs resulted mainly from the fact that the calibration procedures were realized by students while attending three different laboratory classes (see Acknowledgments).

Just as it is in the case of the optical dividing head (the first test rig), the second test rig features a high kinematic precision owing to an accurate integration of the rotary stages into one mechanical structure, in order to avoid various positioning errors discussed, e.g., in [40].

During the experiments, each accelerometer was used separately and measured the Cartesian components of the gravitational acceleration in x-, y-, and z-axes. The calibration procedure enabled determining the parameters of the analog output signals of the accelerometers. The signals can be represented by the following formulas [37]:

$$U_x = o_x + s_x \sin(\alpha + p_x), \tag{1}$$

$$U_y = o_y + s_y \sin\left(\gamma + p_y\right), \tag{2}$$

$$U_z = o_z + s_z \cos(\alpha + p_{z\alpha}), \tag{3}$$

$$U_z = o_z + s_z \cos\left(\gamma + p_{z\gamma}\right), \tag{4}$$

where U_x, U_y, and U_z are the output voltage assigned to x-, y-, or z-axis (V); o_x, o_y, and o_z are the offset of the output

(a)

(b)

Figure 3: The tested accelerometer and the aligning instrument installed in the first test rig: (a) calibration of x- and z-axis; (b) calibration of y- and z-axis.

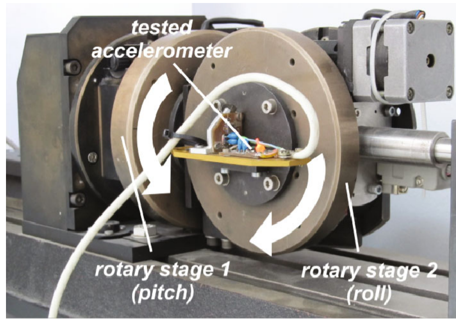

Figure 4: The tested accelerometer installed in the second test rig.

voltage assigned to U_x, U_y, or U_z (V); s_x, s_y, and s_z are the scale factor of the output voltage assigned to U_x, U_y, or U_z (V); p_x, p_y, $p_{z\alpha}$, and $p_{z\gamma}$ are the geometrical phase shift of the output voltage assigned to U_x, U_y, or U_z (deg); α is the pitch applied by means of the test rig (configuration in Figure 3(a) or position of the rotary stage 1 in Figure 4) (deg); and γ is the roll applied by means of the test rig (configuration in Figure 3(b) or position of the rotary stage 2 in Figure 4) (deg).

In the case of studying aging effects related to the offset and the scale factor, the geometrical phase shifts are of no concern. Their value, typically of few tenths of arc degree, results mainly from a random character of mounting the accelerometer PCB in the aligning instrument and then fixing the instrument in the test station. Therefore, the phase shifts have not been analyzed later in the text.

2.3. The Methodology. The following methodology was employed while performing the experimental studies. First, the tested accelerometer was aligned with respect to the rotation axes of the test rig. A fast alignment procedure described by the author in [41] was applied, using the aligning instrument shown in Figure 3 and minutely described in [37]. Then, the output voltages of the accelerometer were obtained as follows.

The output shaft of the optical dividing head (Figure 3) was driven manually, or the computer activated a respective rotary stage (Figure 4); the rotation axis was always horizontal during the tests. When a desired angular position had been set, series of the corresponding output voltages of the tested accelerometer were recorded. While recording the output signal assigned to the x-axis, the configuration shown in Figure 3(a) was used or the rotary stage 1 was powered (pitch angle)—Figure 4, whereas for obtaining the output signal assigned to the y-axis, the configuration shown in Figure 3(b) was used or the rotary stage 2 was put in motion (roll angle)—Figure 4. The output signal assigned to the z-axis was simultaneously recorded in both cases.

Each test consisted in rotating the accelerometers over the full range (360°) of pitch or roll, respectively. In most of the cases, the angular positions were changed with a step of 1° (sometimes, due to lack of time, with a step of 5° exceptionally—see Acknowledgments). At each angular position, when the rotation axis had already reached the desired angular position and was immobile, the accelerometer output voltages were sampled 30 times with the results recorded in the computer memory. So, each calibration consisted of 10,800 records (or 2,160 exceptionally).

In the case of applying the roll angle by means of the rotary stages, each calibration procedure was preceded by calibrating the accelerometers with respect to pitch, in order to precisely find the zero-pitch angle and only then apply pure roll.

In order to determine parameters $o_{x..z}$ and $s_{x..z}$ specified in Equations (1)–(4), i.e., the offsets and the scale factors assigned to each sensitive axis, the recorded data were processed by means of software for statistical analysis (Statgraphics), employing nonlinear regression models fully consistent with Equations (1)–(4). Some researchers, proposed another approach, e.g., in [29, 30, 42], where only extreme indications of the accelerometer are used to

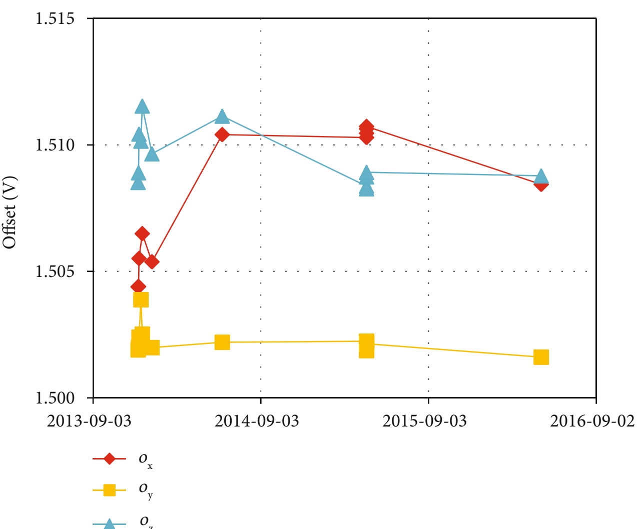

Figure 5: Changes of the offsets of ADXL 330 over time.

determine the aforementioned parameters $o_{x..z}$ and $s_{x..z}$. Our own experiments proved that the parameters determined according to both methods reveal no significant difference in their values. However, as the reported results were obtained while realizing another goal at the same time (tilt measurements), the method of determining only extreme indications of the accelerometer was not used.

3. Results

The graphs presented in Sections 3.1 and 3.2 were created on the basis of the same set of data. It was accepted that the subscripts of the offset $o_{x..z}$ and the scale factor $s_{x..z}$ are consistent with the particular sensitivity axes of the accelerometers. The presented data consist of 21 calibration procedures for ADXL 330, 37 for ADXL 327#1, and 50 for ADXL 327#2, which can be expressed in terms of ca. 54, 100, or 120 hrs of operation, respectively. Only one piece of ADXL 330 was tested, because it was not expected that these accelerometers will cease to operate for no apparent reason. It happened unexpectedly in 2016, and thus, the second piece had been calibrated only a few times in 2015. Since average values of parameters related to particular sensitive axes differ considerably, the ordinate scale is different for each graph (Figures 5–10). Each pair of calibration procedures generated 2 sets of o_z and s_z parameters for z-axis (having almost the same value). So, it was decided to present on the graphs only one set, with values that differed more from their original counterparts.

3.1. Offset. Changes of the offset assigned to each sensitive axis of all the three accelerometers are illustrated in Figures 5–7 over the whole time of testing. It is interesting that only in the case of ADXL 330 the biggest changes occurred at the very beginning (Figure 5). However, it applies only to the offset and not the scale factor (Figure 8). Except for this fact, all the courses have a rather similar character. Differences in the average level of the offsets result from individual properties of each accelerometer.

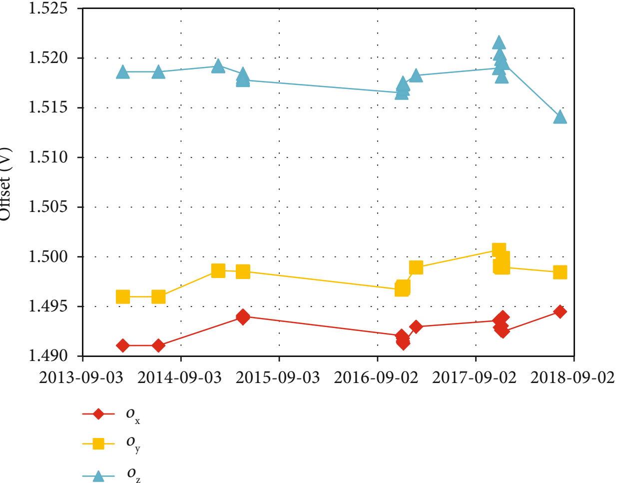

Figure 6: Changes of the offsets of ADXL 327#1 over time.

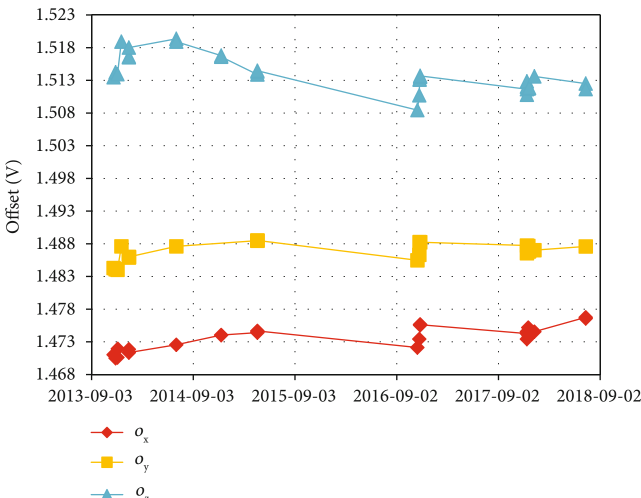

Figure 7: Changes of the offsets of ADXL 327#2 over time.

Generally, the courses corresponding to the offsets have a different character among sensitive axes of a particular accelerometer, as well as among the accelerometers. The existing variations between the sensitive axes and the accelerometers prove that the observed changes originated rather in the tested accelerometers, and not in the measurement circuit.

Maximal absolute and relative (with respect to the value determined most early) changes of the offset observed over the whole time of the experiments are presented in Table 1.

3.2. Scale Factor. The scale factor is usually expressed in volts per g (V/g), e.g., in [27, 29]. Yet, due to introducing Equation (5), which corresponds to the employed calibration procedure employing tilt angles as the reference, it is assumed that this parameter is expressed in volts in Equations (1)–(6), just like the offset.

In general, the courses corresponding to the scale factors have a similar character for sensitive axes of a particular accelerometer, but they differ among the accelerometers. The existing variations between the accelerometers prove

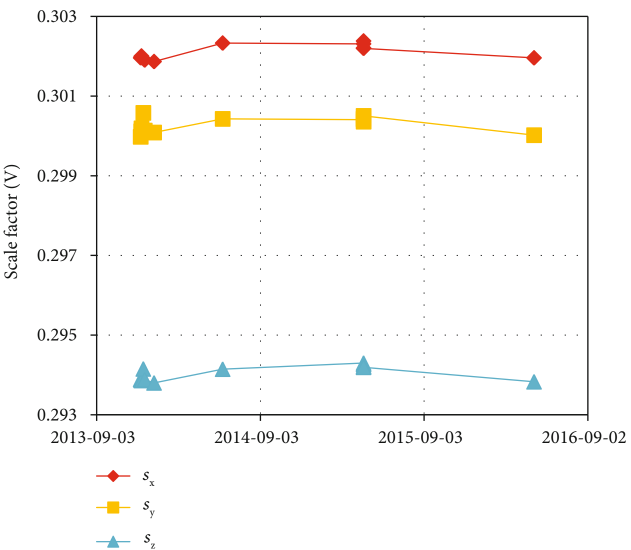

Figure 8: Changes of the scale factors of ADXL 330 over time.

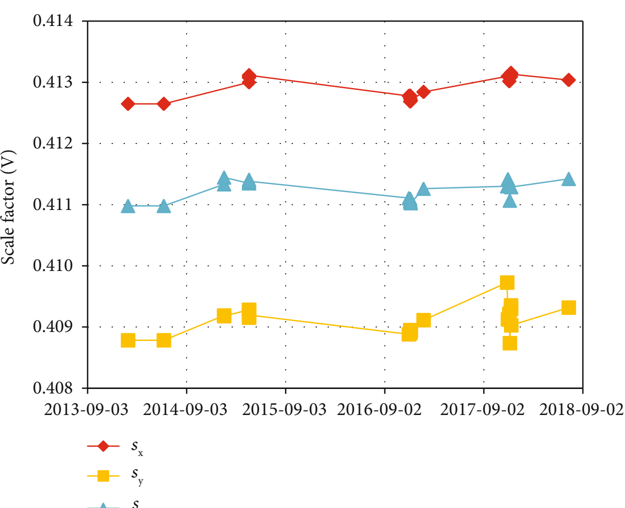

Figure 9: Changes of the scale factors of ADXL 327#1 over time.

that the observed changes originated rather in the tested accelerometers, and not in the measurement circuit.

Maximal absolute and relative (with respect to the value determined most early) changes of the scale factor observed over the whole time of the experiments are presented in Table 2.

In the case of the offset, the absolute changes are of 0.0020–0.0063 V, whereas the absolute changes related to the scale factor vary over a smaller range of 0.0004–0.0009 V. However, since the offset is of a larger magnitude than the scale factor, the relative changes are 0.13%–0.42% and 0.11%–0.23%, respectively.

While determining the considered parameters for each calibration procedure, the value of the respective adjusted *R*-squared coefficient (determination coefficient) was at least of 99.96%, which confirms that the obtained data are of high reliability.

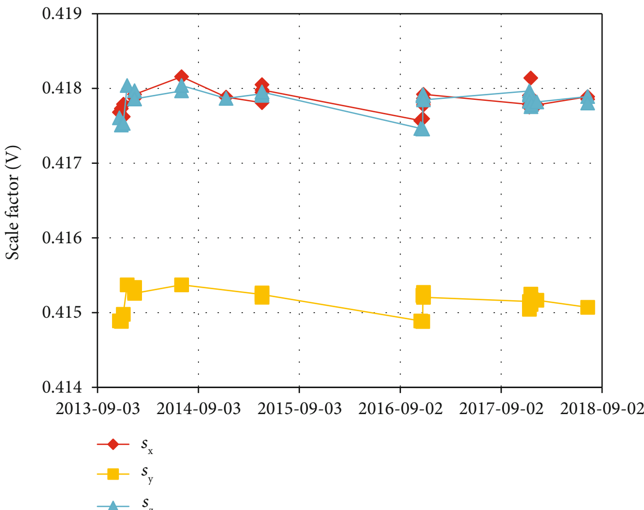

Figure 10: Changes of the scale factors of ADXL 327#2 over time.

Table 1: Maximal changes of the offsets.

Accelerometer	Parameter	Original value (V)	Absolute change (V)	Relative change
ADXL 330	o_x	1.5044	0.0063	0.42%
ADXL 330	o_y	1.5019	0.0020	0.13%
ADXL 330	o_z	1.5085	0.0030	0.20%
ADXL 327#1	o_x	1.4911	0.0034	0.23%
ADXL 327#1	o_y	1.4960	0.0047	0.32%
ADXL 327#1	o_z	1.5186	0.0045	0.30%
ADXL 327#2	o_x	1.4710	0.0057	0.39%
ADXL 327#2	o_y	1.4843	0.0042	0.28%
ADXL 327#2	o_z	1.5135	0.0059	0.39%

3.3. Errors of Determining the Acceleration. In order to determine acceleration a in units of m/s^2 while measured by means of an analog MEMS accelerometer calibrated as aforementioned, the following formula must be applied:

$$a_{x..z} = m_{x..z} \cdot g, \quad (5)$$

where g is the gravitational acceleration (ca. 9.78–9.83 (m/s^2); 9.81 in Warsaw, Poland); $m_{x..z}$ is the relative acceleration in x-, y-, z-axis (respectively) in terms of a multiple of g, computed as

$$m_{x..z} = \frac{U_{x..z} - o_{x..z}}{s_{x..z}}. \quad (6)$$

While determining tilt angles only, like in the case of the employed calibration procedures, $m_{x..z} \in \langle -1, 1 \rangle$, whereas in the case of using the whole measurement range of the tested accelerometers, i.e., (± 3 g) or (± 2 g), $m_{x..z} \in \langle -3, 3 \rangle$ or $m_{x..z} \in \langle -2, 2 \rangle$, respectively.

Table 2: Maximal changes of the scale factors.

Accelerometer	Parameter	Original value (V)	Absolute change (V)	Relative change
ADXL 330	s_x	0.3020	0.0004	0.14%
ADXL 330	s_y	0.3000	0.0006	0.20%
ADXL 330	s_z	0.2938	0.0005	0.16%
ADXL 327#1	s_x	0.4126	0.0005	0.12%
ADXL 327#1	s_y	0.4088	0.0009	0.23%
ADXL 327#1	s_z	0.4109	0.0005	0.12%
ADXL 327#2	s_x	0.4177	0.0005	0.11%
ADXL 327#2	s_y	0.4149	0.0005	0.12%
ADXL 327#2	s_z	0.4175	0.0005	0.13%

Table 3: Absolute and relative maximal errors of the measured acceleration.

Accelerometer	Acceleration	$\Delta m_{x..z}$	$\delta m_{x..z}$	$\delta g_{x..z}$
ADXL 330	m_x	0.0243	0.81%	2.18%
ADXL 330	m_y	0.0126	0.42%	0.86%
ADXL 330	m_z	0.0115	0.38%	1.03%
ADXL 327#1	m_x	0.0152	0.51%	0.92%
ADXL 327#1	m_y	0.0243	0.81%	1.39%
ADXL 327#1	m_z	0.0197	0.66%	1.21%
ADXL 327#2	m_x	0.0220	0.73%	1.42%
ADXL 327#2	m_y	0.0178	0.59%	1.10%
ADXL 327#2	m_z	0.0238	0.79%	1.50%

According to [41], the absolute maximal error of determining the acceleration $\Delta m_{x..z}$ with respect to variations of the offset and the scale factor can be evaluated as

$$\Delta m_{x..z} = c_o \Delta o_{x..z} + c_s \Delta s_{x..z} + c_U \Delta U_{x..z}, \quad (7)$$

where c_o, c_s, and c_U are sensitivity coefficients [39], calculated as follows:

$$c_o = \left| \frac{\partial m_{x..z}}{\partial o_{x..z}} \right| = \frac{1}{s_{x..z}}, \quad (8)$$

$$c_s = \left| \frac{\partial m_{x..z}}{\partial s_{x..z}} \right| = \frac{1}{s_{x..z}} \cdot \frac{|U_{x..z} - o_{x..z}|}{s_{x..z}} = c_o \frac{|U_{x..z} - o_{x..z}|}{s_{x..z}}, \quad (9)$$

$$c_U = \left| \frac{\partial m_{x..z}}{\partial U_{x..z}} \right| = \frac{1}{s_{x..z}} = c_o. \quad (10)$$

As far as evaluation of the accelerometer performance over time is concerned, the most interesting case is when Equation (7) takes on the maximal value. Let us disregard at this point the influence of variations of the output voltage expressed by Equation (10), as not related directly to aging phenomena. So, comparing the sensitivity coefficients c_o and c_s (see Equations (8) and (9)), we see that in order to find relation between them, the value of the following variable v must be analyzed:

$$v = |U_{x..z} - o_{x..z}|. \quad (11)$$

If $v \le s_{x..z}$, then $c_o \ge c_s$, whereas if $v \ge s_{x..z}$, then $c_s \ge c_o$. If the scale factor was determined as corresponding to the full measurement range of the accelerometer, inequality $v \le s_{x..z}$ would be always true. However, in our case, the scale factor corresponds to half or one third of the measurement range, so for accelerations $|a_{x..z}| \le 1\,g$ (e.g., in tilt measurements), expression $c_o \ge c_s$ is true; otherwise, $c_o \le c_s$.

Effects of the maximal changes of the offset and the scale factor on the relative acceleration $m_{x..z}$ are shown in Table 3. While calculating maximal absolute acceleration errors $\Delta m_{x..z}$ and relative acceleration errors $\delta m_{x..z}$, the worst case was assumed, which corresponded to the full measurement range of a particular accelerometer. So, in the case of ADXL 330 with the measurement range (±3 g), it was the case when the maximal value of $U_{x..z}$ was measured, and then $v = 3s_{x..z}$, whereas in the case of ADXL 327 with the measurement range (±2 g), $v = 2s_{x..z}$. Therefore, the analyzed influence of changes of the scale factor was three or two times stronger than that of the offset. Having accepted the aforementioned assumptions, Equation (7) can be rearranged as

$$\Delta m_{x..z} = \frac{1}{s_{x..z}} \left(\Delta o_{x..z} + \frac{v}{s_{x..z}} \Delta s_{x..z} \right). \quad (12)$$

Values of particular relative maximal errors $\delta m_{x..z}$, corresponding to full scales of the tested accelerometers, have been determined in the case of ADXL 330 according to (13) for each calibration procedure.

$$\delta m_{x..z} = \frac{\Delta o_{x..z} + 3\Delta s_{x..z}}{3 s_{x..z}}. \quad (13)$$

In the case of ADXL 327, the relative maximal errors $\delta m_{x..z}$ were computed as follows:

$$\delta m_{x..z} = \frac{\Delta o_{x..z} + 2\Delta s_{x..z}}{2 s_{x..z}}. \quad (14)$$

Values of the errors are illustrated in Figures 11–13, whereas their biggest values are tabulated in Table 3.

Since low-g MEMS accelerometers are often used for tilt measurements, it was decided to additionally determine relative maximal error $\delta g_{x..z}$ related to measurements of components of the gravitational acceleration, employing the following formula:

$$\delta g_{x..z} = \frac{\Delta o_{x..z} + \Delta s_{x..z}}{s_{x..z}}. \quad (15)$$

The biggest values of absolute errors $\Delta m_{x..z}$, their corresponding relative errors $\delta m_{x..z}$ presented in Figures 11–13, and values of the relative errors $\delta g_{x..z}$ are listed in Table 3 for each accelerometer and each sensitive axis.

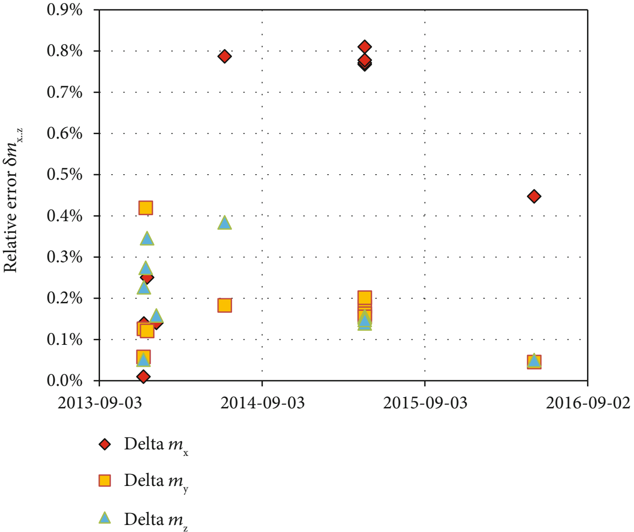

Figure 11: Relative errors for ADXL 330 over time.

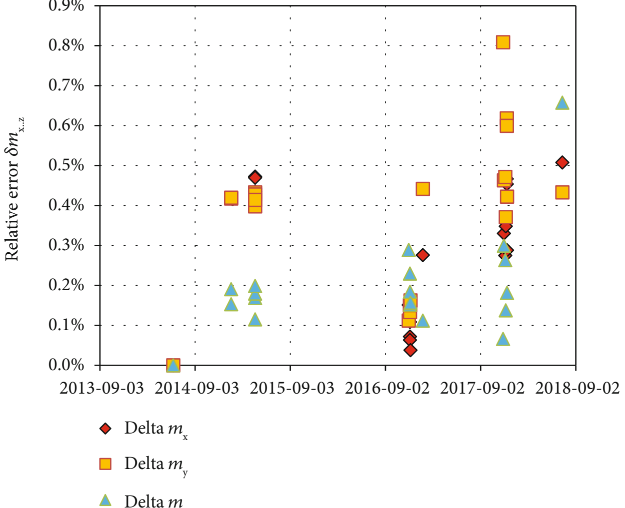

Figure 12: Relative errors for ADXL 327#1 over time.

As it was the case with the changes of the scale factor (Table 2), the errors are similar for all the three sensors; however, perceptible differences exist between sensitive axes of a particular accelerometer.

4. Discussion

Since the studied aging effects involved changes related to many different components, it is hard to explain the character of courses presented in Figures 5–10. However, individual character of some courses (especially those presented in Figures 5–7) and values related to particular sensitivity axes suggest that most of the aging effects took place in the accelerometers themselves.

Changes of the offset are affecting the maximal error a few times more than the changes of the scale factor, especially in the case of tilt measurements, when $|a_{x..z}| \leq 1$ g, and the

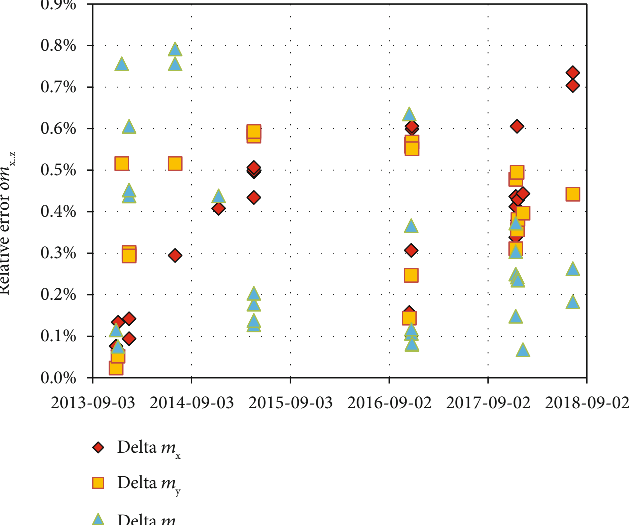

Figure 13: Relative errors for ADXL 327#2 over time.

sensitivity coefficient associated with the offset is bigger than its counterpart associated with the scale factor.

Even though values of errors $\Delta m_{x..z}$ and $\delta m_{x..z}$ listed in Table 3 are of the same magnitude for all the tested accelerometers, only one piece of them (ADXL 327#1) revealed some systematic tendencies in changes of the analyzed parameters that can be attributed to aging: the offset (Figure 6) as well as the scale factor (Figure 9) finally took on values perceptibly different than the original ones; thus, the maximal error (Figure 12) features a tendency to increase its value over time, being insignificant at the beginning of the study. In the case of the other two accelerometers, no increase of the maximal error over time can be observed—-sometimes even the opposite.

As aforementioned, within the time of testing, the data acquisition module was replaced for another one in the case of the second test rig. So, 3 pieces of the module were employed altogether. However, no significant difference in the obtained results was observed, which results also from the fact that all the three modules featured similar accuracy according to the relevant data sheets [35, 38]. Besides, this fact proves that aging effects associated with the modules were rather insignificant, even though the data sheet states that it is guaranteed that the specified absolute accuracy is valid for up to one year from the device external calibration [38]. Considerable difference in precision of applying tilt angles by means of both test rigs (±0.0008° and ±0.02°) was not significant either.

The range of the ambient temperature of 15-40°C, under which the accelerometers were stored, was quite narrow, which may not be the case in many applications, where the main device operates or is stored under more severe conditions. Particularly higher temperatures may be critical, as they speed up the process of aging of MEMS devices [24, 25].

Moreover, there are few other factors that most probably will considerably intensify the aging effects. These are mechanical overloads (including high-g shocks) of the accelerometer both while operated as well as stored (the tested

accelerometers were not overloaded within their whole life), material fatigue of mechanical members of the accelerometer, and longer operation time (the tested accelerometers were operated for no more than 200 hrs). So, it is rather certain that the values of errors related to aging phenomena will be in most of the cases bigger than the reported ones.

Since the absolute accuracy of the data acquisition modules (ca. 0.0015 V) equal the triple value of the observed changes of the scale factor (ca. 0.0005 V), it may be the reason why the graphs in Figures 8–10 are smoother than their counterparts related to the offset (Figures 5–7). However, on the other hand, it must be taken into account that the scale factors, as well as the offsets, were not measured directly but were computed on the basis of appropriate regression models, using huge amounts of data.

Values of the maximal errors related to the sensitive axes of the tested accelerometers (ca. 0.4-0.8%) are smaller than values reported in relevant publications, e.g., 5% in [14] or 2.6% in the case of biaxial MEMS accelerometers [12].

5. Conclusions

The presented study did not investigate particular aging mechanisms but rather enabled an overall evaluation of the aging effects, providing practical information, useful both for the scientific community and engineers employing MEMS accelerometers as measuring instruments rather than detectors.

A considerable decrease of accuracy of triaxial MEMS accelerometers due to natural aging phenomena was determined in terms of changes of the offset and the scale factor associated with each sensitive axis of the accelerometers.

The largest evaluated maximal errors due to aging of the tested accelerometers, the electronic components on the accelerometer PCBs (especially the constant-voltage regulators) are of ca. 0.8%. Therefore, the errors must not be overlooked not only in the case of applications of MEMS accelerometers where a high precision is required (e.g., laboratory measurements) but also if accuracy of ca. 1% is expected to last for a time longer than a few years. This refers specially to control systems directly responsible for human life and safety, like new generation of sophisticated automotive air-bags, motorcycle ABS, or diving computers.

If a MEMS accelerometer is to be applied in systems featuring durability longer than 5 years, either the accelerometer must be recalibrated or a loss in accuracy of its indications must be taken into account.

The observed changes are not of a linear, exponential, or even any systematic character (differences between particular sensitive axes occurred), which makes it rather impossible to create adequate models of aging in order to compensate for the relevant errors. Since the observed changes due to aging related to the offset and the scale factor are of considerable values (and would be definitely bigger under harsher conditions of storing and operation), it is advantageous to repeatedly calibrate the accelerometers. Then, the related errors can be compensated for [11], to some extent of course. Many different calibration procedures have been successfully used so far, some typical, as, e.g., in [43], some quite sophisticated, as, e.g., in [8–10, 44, 45]. Another interesting approach to overcoming the aging effects may be the application of additional sensors, e.g., visual camera, which may be also useful for identification of other failures of a device [46].

Concluding, the following should be stated:

(i) Output signals of only one accelerometer reveal some perceptible aging tendencies, however rather of no monotonic character

(ii) A time period of 4.5 years seems not to be long enough to observe aging effects in the tested triaxial MEMS accelerometers—contrary to what has been observed by the authors in the case of similar biaxial MEMS accelerometers [12] (by the same manufacturer)

(iii) Both pieces of the tested ADXL 330 stopped operating properly after ca. 4.5 years of being used, almost at the same time and for no apparent reason

(iv) The presented research does not address such issues as follows: testing a larger part of a production batch of accelerometers (only 4 pcs were tested); testing and storing the accelerometers under harsh conditions with respect to temperature range, humidity, and mechanical shocks; and operating the accelerometers for a time longer than ca. 120 hrs altogether; under such conditions, the errors due to aging effects will be definitely much bigger

Having encountered the unexpected critical fault of both ADXL 330 accelerometers, a conclusion was reached: since MEMS accelerometers are usually low-cost sensors, in the case of highly reliable systems, it would be advantageous to double the accelerometers or at least frequently activate the self-test function [32, 33] in order to detect any failure.

It is foreseen to continue the study of aging effects in the case of both ADXL 327 accelerometers, which are regularly used by students during laboratory classes, until more significant differences in their operational parameters are recorded.

Data Availability

We are able to provide the data related to our research upon request; however, the files have not been posted on any server.

Conflicts of Interest

The authors declare that they have no conflicts of interest.

Authors' Contributions

Sergiusz Łuczak designed and wrote the manuscript; Maciej Zams created the software controlling the test rig and prepared and analyzed the experimental data; Karol Bagiński revised the manuscript and extended it.

Acknowledgments

The authors would like to thank the students of the Faculty of Mechatronics, Warsaw University of Technology, specializing in micromechanics, for their diligent realization of the experimental works during laboratory classes "Studies of tilt sensors," "Determining mechanical hysteresis of MEMS accelerometers," and "Determining orthogonality errors of the sensitive axes of MEMS accelerometers" within academic years 2013/14–2017/18. The obtained results constitute an essential part of the data used for processing the final results presented in the paper. Moreover, the authors give Ms. Karolina Jarecka credit for preliminary processing of the experimental data. This research was supported by the Faculty of Mechatronics, Warsaw University of Technology under Grant 504/04197/1143/44.000000.

References

[1] C. Yu, N. El-Sheimy, H. Lan, and Z. Liu, "Map-based indoor pedestrian navigation using an auxiliary particle filter," *Micromachines*, vol. 8, no. 7, p. 225, 2017.

[2] C. Dobbins and R. Rawassizadeh, "Towards clustering of mobile and smartwatch accelerometer data for physical activity recognition," *Informatics*, vol. 5, no. 2, p. 29, 2018.

[3] S. Łuczak, "Tilt measurements in BMW motorcycles," in *Recent Global Research and Education: Technological Challenges*, R. Jabłoński and R. Szewczyk, Eds., pp. 287–293, Springer International Publishing, Cham, Switzerland, 2017.

[4] S. Łuczak, R. Grepl, and M. Bodnicki, "Selection of MEMS accelerometers for tilt measurements," *Journal of Sensors*, vol. 2017, Article ID 9796146, 13 pages, 2017.

[5] D. Su, Y. Xia, and R. Yuan, "Self-powered wireless sensor network for automated corrosion prediction of steel reinforcement," *Journal of Sensors*, vol. 2018, Article ID 4125752, 10 pages, 2018.

[6] A. D'Alessandro, A. Meoni, and F. Ubertini, "Stainless steel microfibers for strain-sensing smart clay bricks," *Journal of Sensors*, vol. 2018, Article ID 7431823, 8 pages, 2018.

[7] C. Chen, Z. Wang, Y. Wang, T. Wang, and Z. Luo, "Reliability assessment for PSC box-girder bridges based on SHM strain measurements," *Journal of Sensors*, vol. 2017, Article ID 8613659, 13 pages, 2017.

[8] I. Frosio, F. Pedersini, and N. A. Borghese, "Autocalibration of triaxial MEMS accelerometers with automatic sensor model selection," *IEEE Sensors Journal*, vol. 12, no. 6, pp. 2100–2108, 2012.

[9] T. Dar, K. Suryanarayanan, and A. Geisberger, "No physical stimulus testing and calibration for MEMS accelerometer," *Journal of Microelectromechanical Systems*, vol. 23, no. 4, pp. 811–818, 2014.

[10] A. Olivares, G. Ruiz-Garcia, G. Olivares, J. M. Górriz, and J. Ramirez, "Automatic determination of validity of input data used in ellipsoid fitting MARG calibration algorithms," *Sensors*, vol. 13, no. 9, pp. 11797–11817, 2013.

[11] J. Zhang, Y. Wu, Q. Liu, F. Gu, X. Mao, and M. Li, "Research on high-precision, low cost piezoresistive MEMS-array pressure transmitters based on genetic wavelet neural networks for meteorological measurements," *Micromachines*, vol. 6, no. 5, pp. 554–573, 2015.

[12] S. Łuczak, J. Wierciak, and W. Credo, "Effects of natural aging in biaxial MEMS accelerometers," *IEEE Sensors Journal*(to be published).

[13] V. Kaajakari, *Practical MEMS*, Small Gear Publishing, Las Vegas, NV, USA, 2009.

[14] X. Xiong, Y. L. Wu, and W. B. Jone, "Material fatigue and reliability of MEMS accelerometers," in *Proceedings of the IEEE Int. Symposium on Defect and Fault Tolerance of VLSI Systems*, pp. 314–322, Boston, MA, USA, 2008.

[15] Y. Yang, E. J. Ng, P. M. Polunin et al., "Nonlinearity of degenerately doped bulk-mode silicon MEMS resonators," *Journal of Micromechanics and Microengineering*, vol. 25, pp. 859–869, 2016.

[16] A. Ya'akobovitz and S. Krylov, "Toward sensitivity enhancement of MEMS accelerometers using mechanical amplification mechanism," *IEEE Sensors Journal*, vol. 10, no. 8, pp. 1311–1319, 2010.

[17] V. Mulloni, M. Barbato, and G. Meneghesso, "Long-term lifetime prediction for RF-MEMS switches," *Journal of Micromechanics and Microengineering*, vol. 26, no. 7, article 074004, 2016.

[18] C. H. He, Y. P. Wang, Q. W. Huang et al., "Research on the packaging reliability and degradation models of quality factors for a high vacuum sealed MEMS gyroscope," in *Proceedings of the 2017 19th International Conference on Solid-State Sensors, Actuators and Microsystems (TRANSDUCERS)*, Kaohsiung, Taiwan, 2017.

[19] J. Dhennin, D. Lellouchi, and F. Pressecq, "How to evaluate the reliability of MEMS devices without standards," in *Proceedings of the 2015 Symposium on Design, Test, Integration and Packaging of MEMS/MOEMS (DTIP)*, pp. 1–3, Montpellier, France, 2015.

[20] K. Krupa, C. Gorecki, R. Jóźwicki, M. Józwik, and A. Andrei, "Interferometric study of reliability of microcantilevers driven by AlN sandwiched between two metal layers," *Sensors and Actuators A*, vol. 171, no. 2, pp. 306–316, 2011.

[21] M. Badura, P. Batog, A. Drzeniecka-Osiadacz, and P. Modzel, "Evaluation of low-cost sensors for ambient $PM_{2.5}$ monitoring," *Journal of Sensors*, vol. 2018, Article ID 5096540, 16 pages, 2018.

[22] D. M. Tanner, J. A. Walraven, M. T. Dugger et al., "Accelerating aging failures in MEMS devices," in *Proceedings of the IEEE International 43rd Annual Reliability Physics Symposium*, pp. 317–324, San Jose, CA, USA, 2005.

[23] H. R. Shea, "Reliability of MEMS for space applications," in *SPIE 6111, Reliability, Packaging, Testing, and Characterization of MEMS/MOEMS V, Proceedings of the MOEMS-MEMS 2006 Micro and Nanofabrication*, pp. 61110A–611110, San Jose, CA, USA, 2006.

[24] F. Schneider, T. Fellner, J. Wilde, and U. Wallrabe, "Mechanical properties of silicones for MEMS," *Journal of Micromechanics and Microengineering*, vol. 18, no. 6, article 065008, 2008.

[25] S. Habibi, S. J. Cooper, J. M. Stauffer, and B. Dutoit, "Gun hard inertial measurement unit based on MEMS capacitive accelerometer and rate sensors," in *Proceedings of the IEEE/ION Position, Location and Navigation Symposium*, pp. 232–237, Monterey, CA, USA, 2008.

[26] M. Barbato, A. Cester, and G. Meneghesso, "Viscoelasticity recovery mechanism in radio frequency

microelectromechanical switches," *IEEE Transactions on Electron Devices*, vol. 63, no. 9, pp. 3620–3626, 2016.

[27] M. Šipoš, P. Pačes, J. Roháč, and P. Nováček, "Analyses of triaxial accelerometer calibration algorithms," *IEEE Sensors Journal*, vol. 12, no. 5, pp. 1157–1165, 2012.

[28] S. Bütefisch, A. Schoft, and S. Büttgenbach, "Three-axes monolithic silicon low-g accelerometer," *Journal of Microelectromechanical Systems*, vol. 9, no. 4, pp. 551–556, 2000.

[29] W. T. Ang, P. K. Khosla, and C. N. Riviere, "Nonlinear regression model of aLow-g MEMS accelerometer," *IEEE Sensors Journal*, vol. 7, no. 1, pp. 81–88, 2007.

[30] W. T. Latt, K. C. Veluvolu, and W. T. Ang, "Drift-free position estimation of periodic or quasi-periodic motion using inertial sensors," *Sensors*, vol. 11, no. 6, pp. 5931–5951, 2011.

[31] C. Acar and A. Shkel, "Experimental evaluation and comparative analysis of commercial variable-capacitance MEMS accelerometers," *Journal of Micromechanics and Microengineering*, vol. 18, pp. 634–645, 2003.

[32] *Small, low power, 3-axis ±3 g iMEMS® accelerometer, ADXL330*, Analog Devices Inc, Norwood, MA., 2007, https://www.analog.com/media/en/technical-documentation/data-sheets/ADXL330.pdf.

[33] *Small, low power, 3-axis ±2 g accelerometer, ADXL327*, Analog Devices Inc., Norwood, MA., 2009, https://pdf1.alldatasheet.com/datasheet-pdf/view/300952/AD/ADXL327.html.

[34] S. Łuczak, "Experimental studies of hysteresis in MEMS accelerometers: a commentary," *IEEE Sensors Journal*, vol. 15, no. 6, pp. 3492–3499, 2015.

[35] S. Łuczak, "Dual-axis test rig for Mems tilt sensors," *Metrology and Measurement Systems*, vol. 21, no. 2, pp. 351–362, 2014.

[36] S.-S. Yun, D.-H. Jeong, S.-M. Wang et al., "Fabrication of morphological defect-free vertical electrodes using a (1 1 0) silicon-on-patterned-insulator process for micromachined capacitive inclinometers," *Journal of Micromechanics and Microengineering*, vol. 19, no. 3, p. 035025, 2009.

[37] S. Łuczak, "Effects of misalignments of MEMS accelerometers in tilt measurements," in *Mechatronics 2013. Recent Technological and Scientific Advances*, T. Brezina and R. Jabłoński, Eds., pp. 393–400, Springer International Publishing, Cham, Switzerland,, 2014.

[38] *USB-6211 Specifications - National Instruments*August 2019, http://www.ni.com/pdf/manuals/375195d.pdf.

[39] *Expression of the uncertainty of measurement in calibration, Publication Reference EA-4/02.*, European Co-operation for Acreditation, 1999.

[40] M. Bodnicki and S. Łuczak, "Comments on "Delay compensation of tilt sensors based on MEMS accelerometer using data Fusion Technique"," *IEEE Sensors Journal*, vol. 18, no. 3, pp. 1333–1335, 2018.

[41] S. Łuczak, "Fast alignment procedure for MEMS accelerometers," in *Advanced Mechatronics Solutions*, R. Jabłoński and T. Brezina, Eds., pp. 481–487, Springer International Publishing, Cham, Switzerland, 2016.

[42] S. Stančin and S. Tomažič, "Time- and computation-efficient calibration of MEMS 3D accelerometers and gyroscopes," *Sensors*, vol. 14, no. 8, pp. 14885–14915, 2014.

[43] Z. Li, W. Wu, P. Zheng, J. Liu, J. Fan, and L. Tu, "Novel capacitive sensing system design of a microelectromechanical systems accelerometer for gravity measurement applications," *Micromachines*, vol. 7, no. 9, p. 167, 2016.

[44] K. Parsa, T. A. Lasky, and B. Ravani, "Design and implementation of a mechatronic, all-accelerometer inertial measurement unit," *IEEE/ASME Transactions on Mechatronics*, vol. 12, no. 6, pp. 640–650, 2007.

[45] Z. F. Syed, P. Aggarwal, C. Goodall, X. Niu, and N. el-Sheimy, "A new multi-position calibration method for MEMS inertial navigation systems," *Measurement Science and Technology*, vol. 18, no. 7, pp. 1897–1907, 2007.

[46] A. Suarez, G. Heredia, and A. Ollero, "Cooperative virtual sensor for fault detection and identification in multi-UAV applications," *Journal of Sensors*, vol. 2018, Article ID 4515828, 19 pages, 2018.

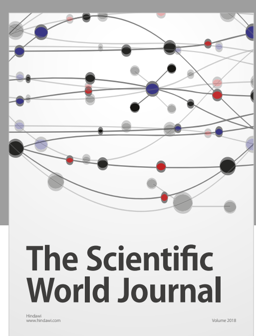

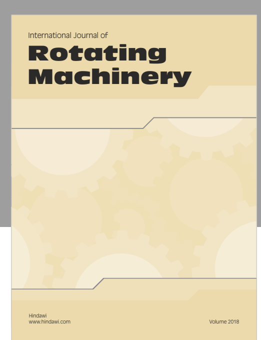

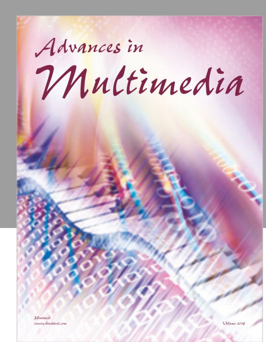

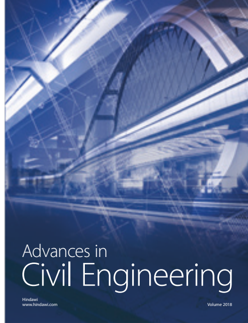

Submit your manuscripts at
www.hindawi.com